LANGMUIR

pubs.acs.org/Langmuir Article

Binding Kinetics of Self-Assembled Monolayers of Fluorinated Phosphate Ester on Metal Oxides for Underwater Aerophilicity

Anca Mazare,* Mahmut Hakan Ulubas, Hyesung Kim, Iana Fomicheva, George Sarau, Silke H. Christiansen, Wolfgang H. Goldmann, and Alexander B. Tesler*

Cite This: *Langmuir* 2025, 41, 1868–1875 Read Online

ACCESS | Metrics & More | Article Recommendations | Supporting Information

ABSTRACT: The term "aerophilic surface" is used to describe superhydrophobic surfaces in the Cassie–Baxter wetting state that can trap air underwater. To create aerophilic surfaces, it is essential to achieve a synergy between a low surface energy coating and substrate surface roughness. While a variety of techniques have been established to create surface roughness, the development of rapid, scalable, low-cost, waste-free, efficient, and substrate-geometry-independent processes for depositing low surface energy coatings remains a challenge. This study demonstrates that fluorinated phosphate ester, with a surface tension as low as 15.31 mN m^{-1}, can form a self-assembled monolayer on metal oxide substrates within seconds using a facile wet-chemical approach. X-ray photoelectron spectroscopy was used to analyze the formed self-assembled monolayers. Using nanotubular morphology as a rough substrate, we demonstrate the rapid formation of a superhydrophobic surface with a trapped air layer underwater.

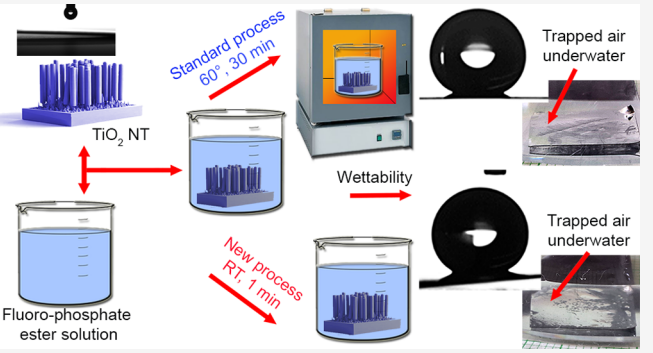

INTRODUCTION

Aerophilic surfaces constitute a special class of materials, characterized by their ability to trap thin films of air underwater, known as plastrons.[1−4] The premise of plastrons is to minimize the contact of solid surfaces with surrounding fluids. Gaining aerophilic surface capabilities to solid materials would be beneficial in several areas, including biomedical devices to reduce contact with blood,[5] and bacterial adhesion,[6] but also providing thermal insulation to maintain body temperature in cold waters.[7] In marine engineering, aerophilicity prevents colonization by aquatic organisms,[8] corrosion of metals,[8,9] and the damage of in-water and underwater structures,[10] to name but a few. Despite extensive research in the field of superhydrophobic/aerophilic surfaces, current achievements in this field are insufficient to meet industrial requirements.[11] To emphasize - air plastron, trapped on an engineered low-energy surface, is a defining feature that enhances surface resilience to detrimental wetting-related phenomena.

To create an aerophilic surface, two conditions should be fulfilled: (*i*) design and fabrication of a solid surface with hierarchical morphologies consisting of micro- and nano-features, and (*ii*) low surface energy coatings that repel water.[12] Fulfilling these conditions results in high water contact angles, typically greater than 150°, and low roll-off angles, typically less than 5°.[13] During the past few decades, various approaches have been developed to increase high surface roughness of solid materials, including mechanical, optical, chemical, and electrochemical.[14−16] The main chemical compounds used to reduce surface energy are fluoropolymers, polyfluoroalkyls, fluorosilanes and fluorinated alkanes, silicones, silane, siloxane, and hydrocarbon-based compounds.[14,17,18] While various surface functionalization approaches have been established and widely explored, the existing methods share several common limitations such as complicated, time-consuming, destructive, and expensive processes, which substantially hinder the widespread use of superhydrophobic surfaces in practical applications.[11] Despite the variety of low surface energy compounds and functionalization approaches, the development of rapid, efficient, easily scalable, cost-effective, and waste-free processes for the deposition of low-surface energy coatings remains a challenge.

TiO_2 is an oxide that is capable of forming surface hydroxyls as exposed to moisture. Typically, headgroups such as chlorosilanes (R_nSiCl_{4-n}, n = 1, 2, 3), alkoxysilanes ($R_nSi(OR')_{4-n}$, n = 1, 2, 3), and carboxylic acids are used to link the solid surface to the organic and fluorinated tails. However,

Received: October 29, 2024
Revised: January 6, 2025
Accepted: January 7, 2025
Published: January 15, 2025

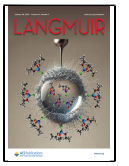

https://doi.org/10.1021/acs.langmuir.4c04320
Langmuir 2025, 41, 1868−1875

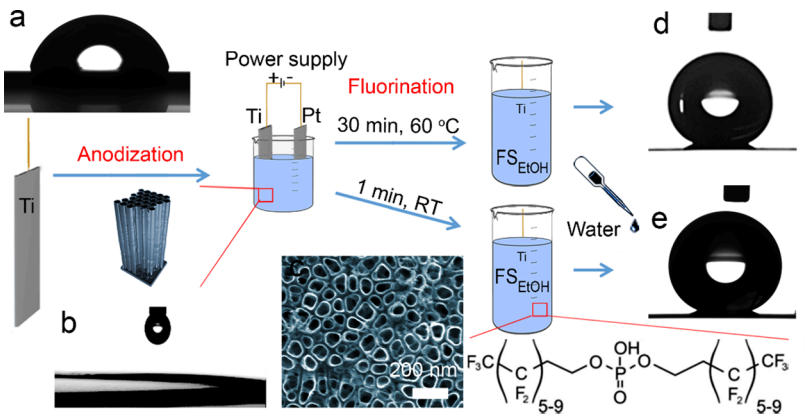

Figure 1. Schematic representation of binding kinetics on the TiO_2 nanotubular array substrates. (a) The water contact angle was measured on the bare Ti substrate. (b) The water contact angle was measured on the as-formed TiO_2 nanotubular arrays. (c) Top-view SEM image of typical TiO_2 NT arrays. Water contact angle after the functionalization with the fluorinated phosphate ester surfactant for (d) 30 min at 60 °C and (e) 1 min at room temperature.

silanes are known to be capable of cross-linking by having at least three leaving groups.[19] Furthermore, silanes with the capacity for cross-linking form self-assembled monolayers with low surface coverage, suggesting island-like film growth.[20] These factors render the process of reducing the energy of solid surfaces complex, inefficient, and challenging to scale up. At the same time, compounds based on phosphonic acid headgroups, which are incapable of cross-linking, have been shown to form highly ordered self-assembled monolayers with high surface coverage, suggesting a uniform film growth mechanism.[19,20] Nevertheless, phosphate-based compounds have been less studied in the context of reducing the surface energy of solid materials.

In this study, we demonstrate that a phosphate ester with a mixed length of fluorinated alkyl chain surfactant (FS) forms a self-assembled monolayer on metal oxide substrates within seconds. When the rough TiO_2 nanotubular (NT) arrays were immersed for only 1 s at room temperature in the FS solution, cleaned, dried, and subsequently submerged in water, these samples exhibited the trapping of an air layer. Furthermore, the immersion of the NT arrays in the FS solution at room temperature for periods exceeding 1 min results in the formation of aerophilic surfaces in underwater environments.

MATERIALS AND METHODS

Materials. Titanium foil with a thickness of 125 μm and a purity of 99.6% was purchased from Advent, Oxford, UK. Phosphate ester of the mixed length of fluorinated alkyl chains surfactant ($(CF_3$-$(CF_2)_{5-9}$-$(CH_2)_2$−$O)_2$-POOH, FS-100, hereafter abbreviated as FS) was purchased from Chemguard, USA. Hydrofluoric acid, sodium dihydrogen phosphate dihydrate, acetone, and ethanol were purchased from Carl Roth, Germany. All chemicals were analytical-grade reagents and were used as received. Deionized (DI) water (18.2 MΩ · cm) was used in all experiments (ELGA, Purelab Ultra, UK).

Anodic TiO_2 Nanotubes. Titanium foil with a thickness of 0.125 mm and a purity of 99.6% (Advent, Oxford, UK) was used for the anodization process. The substrates were ultrasonically cleaned in acetone and ethanol for 10 min each. Subsequently, the anodization was performed in an electrolyte consisting of 1 M $NaH_2PO_4 \times 2H_2O$ and 0.125 M HF at an applied voltage of 20 V for 2 h. After anodization, the samples were immersed in distilled water for 30 min to remove residual chemicals, ultrasonicated in water for 10 min, and then dried in a stream of N_2.[21]

Deposition of 80 nm Thick TiO_2 Films. The flat 80 nm think TiO_2 layers were formed on Si wafer supports by reactive direct current magnetron sputtering (DC-MS, Createc, SP-P-US-6M-3Z) method using a pure Ti (99.995%, HMW-Hauner GmbH & Co. KG) as a sputtering target. First, a thin Ti interlayer was sputtered on clean Si wafer substrates at 150 W DC power. Subsequently, 80 nm thick TiO_2 was sputtered at 500 W DC power and 6.7×10^{-3} mbar pressure under an Ar/O_2 (volume ratio 2:1) atmosphere controlled by mass flow controllers (MFC, MKS Instruments, Inc.).

Surface Modification with Fluorinated Phosphate Ester. The surfactant, phosphate ester with a mixed length of fluorinated alkyl chains (FS-100, $\gamma = 15.31 \pm 0.33$ mN m^{-1}), (10 g) was dissolved in 1 L of 95:5 vol % ethanol: H_2O by ultrasonication and then kept in a closed container under ambient conditions. The samples were immersed in the surface modifier solution. A plastic cover to prevent ethanol evaporation was used to seal the surfactant container. A container containing the high surface roughness samples was placed in a muffle furnace preheated to +60 °C for 30 min. The low surface energy metallic substrates were then rapidly removed from the surface modifier solution (a typical speed of removal is ∼50 mm s^{-1}), rinsed with ethanol, and dried under a stream of N_2. Alternatively, the samples were immersed in the container of the surface modifier solution for 1 s, 1 min, and 5 min at room temperature. The low surface energy substrates were then rapidly removed from the surface modifier solution, rinsed with ethanol, and dried under a stream of N_2.

Physicochemical Characterization. The morphology of the flat or the TiO_2 nanotube layers, reference (bare) was investigated by field-emission scanning electron microscopy (FE-SEM, Hitachi S4800). The nanotube layer was mechanically scratched to evaluate the cross-section. The chemical composition of the flat or TiO_2 nanotube layers, with or without the FS functionalization was evaluated by X-ray photoelectron spectroscopy (XPS, PHI 5600, US). The TiO_2 samples were mounted on the sample holder and introduced into the ultrahigh vacuum chamber. Survey and high-resolution scans were performed to obtain detailed spectra of the core-level electrons, for the latter for C 1s, O 1s, Ti 2p, F 1s, and P 2p. Note that the spectra were calibrated with the Ti 2p peak at 459.0 eV and that peak fitting was performed in the Multipak software (version 9.9.0.19).

Surface Roughness. The roughness of the magnetron-sputtered flat TiO_2 layers deposited on the Si wafer and rough NT arrays were measured using confocal laser microscopy DCM 3D (Leica Inc., Germany) that combines confocal and interferometry technology having resolution measurements down to 0.1 nm. The measurements were performed using the x50 objective. The 201 slices were measured with a step size of 0.2 μm. The topography images were then characterized by Gwyddion 2.65 software to calculate the average (R_a) roughness.

Attenuated Total Reflectance Fourier Transform Infrared Spectroscopy. A Cary 660 FTIR spectrometer (Agilent Technol-

https://doi.org/10.1021/acs.langmuir.4c04320
Langmuir 2025, 41, 1868−1875

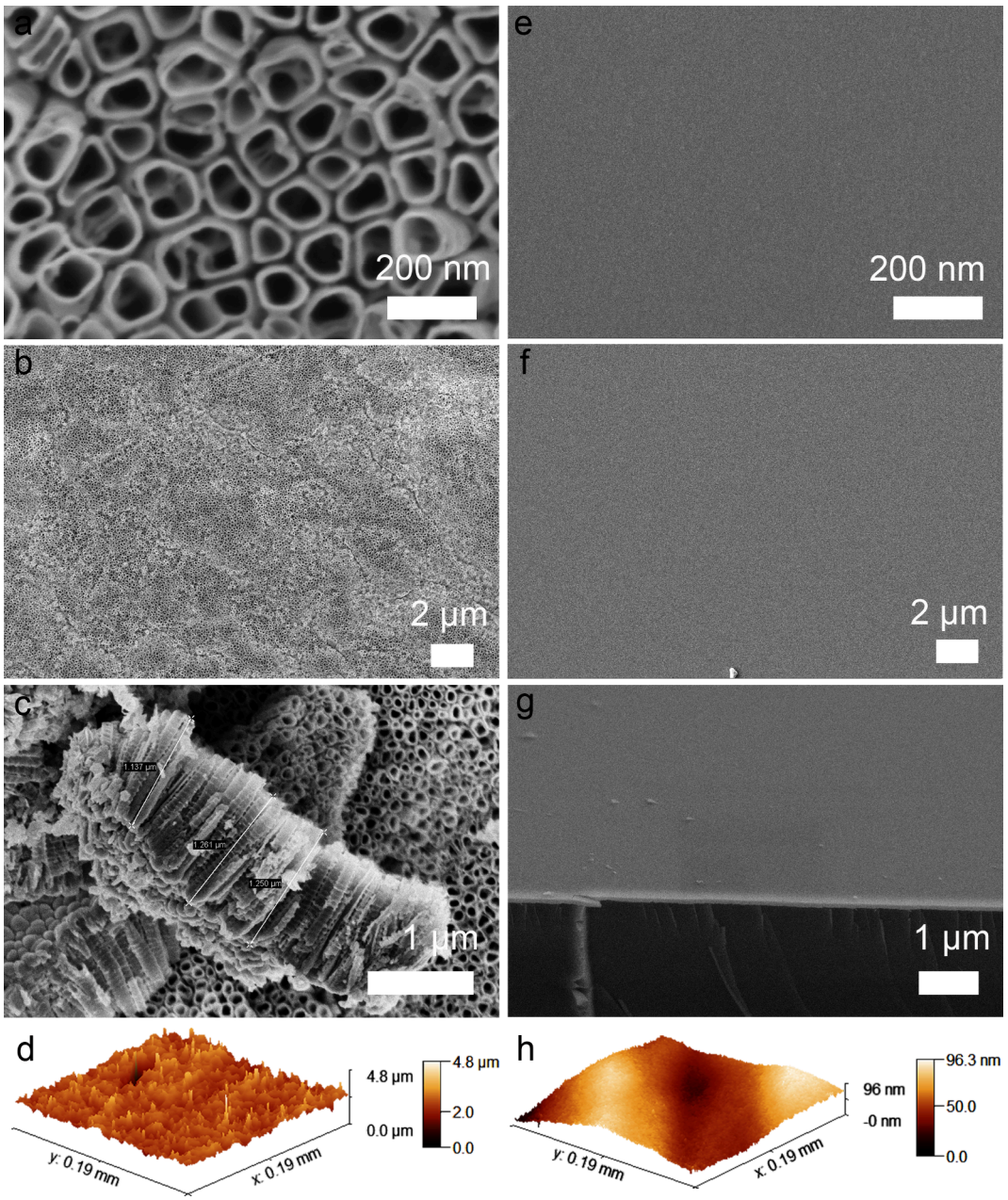

Figure 2. High-resolution SEM and 3D reconstruction of confocal laser microscopy images of (a–d) the anodized TiO_2 nanotube arrays and (e–h) magnetron sputtered TiO_2 flat film on Si wafer.

ogies, Germany) was used in Single Point Reflection mode. FTIR spectra were recorded in the range between 4000–400 cm^{-1} with 16 scans and at a resolution of 2 cm^{-1}. The free IR beam in the air was measured immediately before the sample and used as background.

Contact Angle Goniometry. Water contact angle measurements were performed at room temperature using a contact angle goniometer (DSA25, KRÜSS, Germany). A 5 μL drop volume of deionized water (DI, 18.2 MΩ·cm) was dropped on the surface. The drop profile image was captured by a camera and then analyzed by the KRÜSS ADVANCE program provided by KRÜSS, employing the sessile drop shape and Laplace–Young fitting method. The surface free energy was estimated using the Owens–Wendt–Rabel–Kaelble (OWRK) method with water and diiodomethane as the polar and disperse fractions of the surface free energy.[22] For CA hysteresis, the drop volume of 30 μL was increased and decreased at a rate of 0.4 μL s^{-1}, and a video was recorded. Fitting was performed using the Ellipse method (Tangent-1) with KRÜSS ADVANCE software. All values in the text were averaged from at least three independent measurements.

Air Plastron Measurements. Air plastron measurements were performed by capturing digital images of the aerophilic TiO_2 NT arrays immersed in a Petri dish filled with DI water at the grazing angle. An optical microscope was used in reflectance mode to determine the presence, shape, and surface coverage of the plastron. The surface tension of the FS was measured by the pendant drop method using a KRÜSS DSA25 contact angle goniometer (KRÜSS, Germany).

RESULTS AND DISCUSSION

A schematic depiction of the coating process is shown in Figure 1. We used closely packed TiO_2 nanotubular arrays (NTs) as rough substrates,[23] while magnetron sputtered thin flat TiO_2 films were used as control, especially to analyze the self-assembled FS monolayers by X-ray photoelectron spectroscopy (XPS). The TiO_2 NTs were obtained by electrochemical anodization in an aqueous electrolyte, and their

https://doi.org/10.1021/acs.langmuir.4c04320
Langmuir 2025, 41, 1868–1875

morphology consisted of 100 nm tube diameter and 1.3 μm tube length (Figure 2a–c). The average roughness (R_a) was determined by confocal laser microscopy and was found to be of the order of 100 nm (Figure 2d).

To reduce the surface energy of metal oxide substrates, the samples were immersed in a bath consisting of 1 wt % FS dissolved in a 95:5 vol % ethanol/water solution (see the chemical formula of FS in Figure 1, inset). The surface tension of the FS solution was determined by goniometric measurements using the pendant drop technique and was found to be γ = 15.31 ± 0.33 mN m^{-1}. Note that polyfluoroalkyl and perfluoroalkyl substances are regulated due to their chemical stability;[24] therefore, to minimize waste of fluorinated compounds, the FS solution was repeatedly used for over 5.5 years without any degradation in coating performance.

The bare Ti substrates exhibit hydrophilic surface characteristics, as indicated by a water contact angle (WCA) of 78.8° ± 1.8° (Figure 1a) and the surface free energy (SFE) of 44.4 ± 1.3 mN m^{-1}. Notably, Ti is a high surface energy material that rapidly forms a native oxide film (up to 10 nm thick) when exposed to atmospheric air. This relatively high WCA is attributed to airborne hydrophobic impurities, which is in agreement with the literature.[23,25−27] We have previously developed a surface fluorination method, in which the solid substrates are typically immersed in a FS solution for 30 min at 60 °C to form a FS self-assembled monolayer, and when applied to rough substrates, the formation of aerophilic surfaces has been observed underwater.[6,9,12,28] However, the binding kinetics of the FS to metal oxide surfaces has not been investigated.

After anodization, the TiO_2 NTs exhibit superhydrophilic properties, with a WCA of approximately 0°, which is below the detection limit of the goniometer (Figure 3a). Subsequently, the anodized TiO_2 NT arrays were immersed in the FS solution for 1 s, 1 min, and 5 min at room temperature (RT), and for 30 min at 60 °C, which served as a control. The samples were then thoroughly rinsed with ethanol and dried. The WCA, contact angle hysteresis (CAH), and SFE were determined for the fluorinated TiO_2 NTs and were found to be 124.3° ± 15.4° (CAH = 50.2° ± 5.0°, SFE = 24.0 ± 1.7 mN m^{-1}), 159.1° ± 6.2° (CAH = 37.6° ± 6.4°, SFE = 17.5 ± 1.6 mN m^{-1}), 162.6° ± 3.0° (CAH = 28.0° ± 6.8°, SFE = 19.4 ± 2.2 mN m^{-1}), and 161.5° ± 3.2° (CAH = 33.5° ± 7.8°, SFE = 15.2 ± 1.48 mN m^{-1}) for 1 s, 1, and 5 min at RT, and 30 min at 60 °C, respectively (Figure 3b–e). The bare and fluorinated TiO_2 NT samples were then immersed in water and images were captured at a grazing angle and by optical reflectance microscopy to detect the formation of plastron. As expected, there is no air entrapment on the as-anodized TiO_2 NTs, which are superhydrophilic (Figure 3f,k). After 1 s immersion at RT, a number of discrete air pockets were already observed (Figure 3g,l). The latter indicates that even after 1 s of immersion in the FS solution at RT, a certain amount of FS molecules is already attached chemically to the TiO_2 surface. For longer immersion times, either at RT or at 60 °C, there is a slight variation in the measured WCA and water affinity of the fluorinated TiO_2 NT samples (Figure 3c–e, and Movie S1). The presence of the FS on TiO_2 NTs was confirmed by attenuated total reflectance Fourier-transform infrared (ATR-FTIR) spectroscopy analysis. The FTIR spectra within the wavenumber range of 400–4000 cm^{-1} are presented in Figure 3p. The distinct peaks at 1150 and 1206 cm^{-1} are indicative of C–F stretching vibrations,[29,30] while one at 1246 cm^{-1} is

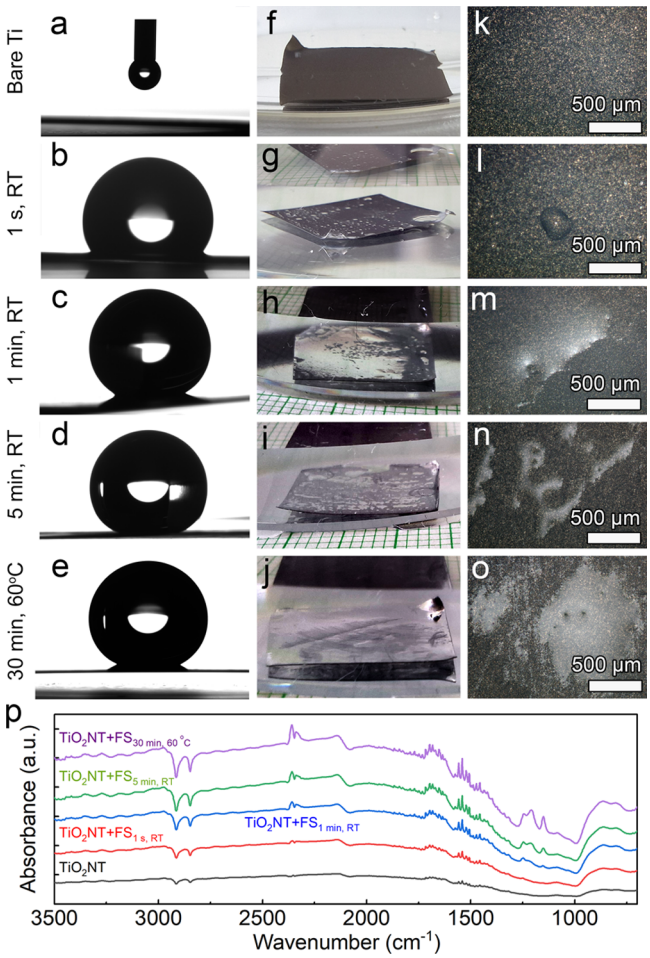

Figure 3. (a–e) Water contact angle measured on the TiO_2 nanotubular array substrates before (a) and after the immersion in the FS solution for 1 s (b), 1 min (c), 5 min (d) at room temperature, as well as 30 min at 60 °C (e). (f) Digital image of the TiO_2 NT substrate immersed in water. (g–j) Digital images of the TiO_2 NT substrates after the immersion in the FS solution for 1 s (l), 1 min (m), 5 min (n) at room temperature, as well as 30 min at 60 °C (o). The images were captured at a grazing angle, while the sample was immersed in water. (k–o) Optical microscopy images of the TiO_2 NT substrates before (k), and after the immersion in the FS solution for 1 s (l), 1 min (m), 5 min (n) at room temperature, as well as 30 min at 60 °C (o). The samples were immersed in water. (p) Fourier transform infrared spectra of the bare TiO_2 NT arrays and after immersion in the FS solution for 1 s, 1 min, and 5 min at RT, and 30 min at 60 °C.

attributed to P = O stretching vibrations of the FS.[31] These peaks are evident already after 1 min of immersion, while the spectra of the samples coated for 5 min at RT, and 30 min at 60 °C are comparable. Moreover, a comparative analysis of the CH_2 stretching vibrations reveals a notable shift in the peak positions. Specifically, the peaks at 2848 and 2915 cm^{-1} in the bare TiO_2 NTs shift to 2849 and 2917 cm^{-1} in the FS-coated sample (Figure S1). This shift is indicative of the substitution of airborne impurities with ordered FS monolayers.[32] The latter results may explain the presence of an air plastron covering a significant part of the sample surface in all FS-coated samples for more than 1 min, irrespective of the deposition temperature (Figure 3h–j,m–o).

However, there are variations in the developed plastrons; therefore, XPS was employed to study the binding kinetics of

https://doi.org/10.1021/acs.langmuir.4c04320
Langmuir 2025, 41, 1868−1875

the FS on the flat and nanotubular TiO_2 surface together with WCA measurements, for different immersion times in the FS solution (see surveys in Figure S2). Selected high-resolution XPS spectra are shown in Figure 4a−c for flat and Figure 4i−k

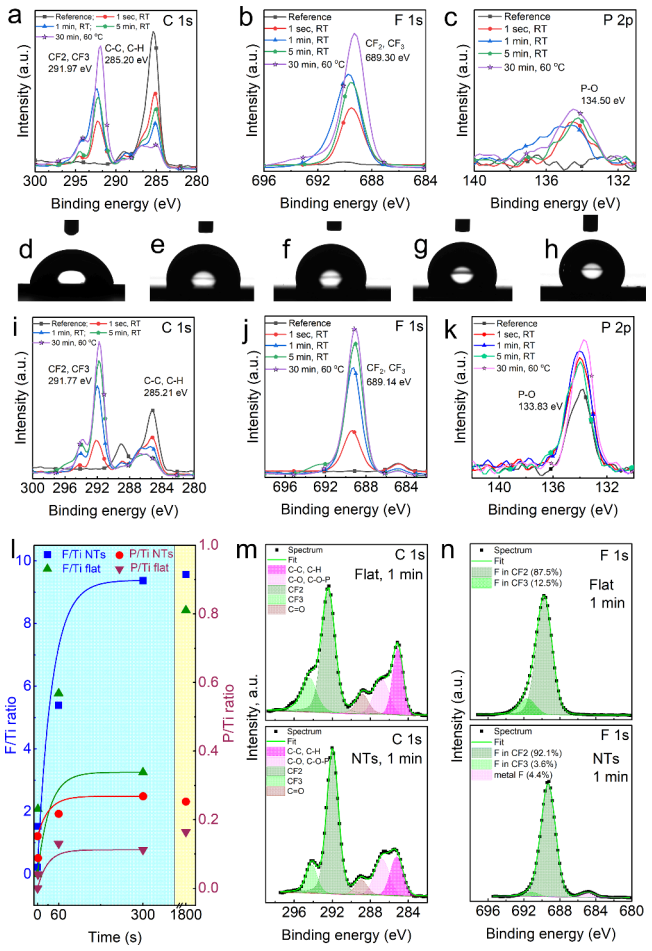

Figure 4. (a−c) High-resolution XPS peaks of the FS-decorated morphologies focusing on C 1s, F 1s, and P 1s, for the reference (bare), 1 s, 1 min, 5 min, or 30 min* (the 30 min treatment was performed at 60 °C) measured on flat TiO_2 layers. (d−h) The water contact angle was measured on flat TiO_2 layers for the reference (bare), 1 s, 1 min, 5 min, or 30 min* (the 30 min treatment was performed at 60 °C). (i−k) High-resolution XPS peaks of the FS-decorated morphologies focusing on C 1s, F 1s, and P 1s, for the reference (bare), 1 s, 1 min, 5 min, or 30 min* (the 30 min treatment was performed at 60 °C) measured on the TiO_2 NT arrays. (l) Overview of the F/Ti and P/Ti ratios, as obtained from the XPS chemical composition data. (m, n) Peak fitting of the C 1s and F 1s peaks for the flat and NT layer after 1 min FS decoration.

for NTs, respectively, for C 1s, F 1s, and P 2p (while those of O 1s and Ti 2p are listed in Figure S3). The magnetron-sputtered flat TiO_2 layers have an average roughness (R_a) value in the order of 1 nm (SEM images in Figure 2e−g and confocal laser microscopy images, Figure 2h) and are thus ideal for XPS measurements to evaluate the binding of FS. The WCA images are shown in Figure 4d−h. Note that the bare flat TiO_2 layers consist only of C, O, and Ti with the C 1s peak centered at ≈285.2 eV, typical of adventitious carbon, which can be attributed to the C−C bonds and C−H adsorbed on the surface. The latter explains the relatively high WCA of the bare TiO_2 layer (Figure 4d). It is noteworthy that the F and P content in the flat layers is zero, and this is significant because the FS functionalization contains C, O, F, and P (with 10−18 CF_2 groups, 2 CF_3 groups, and PO groups); therefore, the evaluation of the C 1s, F 1s, and P 2p peaks is crucial. In the case of the bare NT layers, the NTs additionally contain F and P as uptake from the anodizing electrolyte (F 1s peak at ≈684.8 eV corresponding to metal fluorides, and P 2p at ≈133.8 eV to phosphate groups).[21,33] Given this initial F and P content in the bare NTs layers (3.71 at% F and 2.55 at% P), to better evaluate the amount of F or P attributed to the FS, we also calculated the F/Ti or P/Ti ratios from the atomic percentage data obtained from XPS (Figure 4l and Tables S1 and S2).

For both the flat and NTs layers, we observe the appearance and increase of the peak at ≈292 and the shoulder at ≈294 eV, typical for CF_2 and CF_3, and the F 1s at ≈689 eV, with increasing the RT treatment time or with the 30 min treatment at 60 °C. Similarly, for the flat layers, we observe the P 2p at ≈134 eV, while for the NTs, since a P 2p is already present in the bare NTs, we observe an increase in the intensity of the peaks. In addition, we also observe a decrease in the Ti 2p and O 1s, which coincides with the increase observed in the aforementioned peaks, further supporting the decoration of the TiO_2 surface with the FS monolayer. The O 1s and Ti 2p peaks (Figure S4), show the typical peaks corresponding to TiO_2:[33,34] for O 1s, a strong peak around ≈530.5 eV, typical for TiO_2, together with a shoulder at ≈532 eV (which can be attributed to −OH, CO bonds and adsorbed water), and for Ti, the $2p_{3/2}$ peak around ≈459 eV, corresponding to Ti^{4+} in TiO_2. The XPS results explain the gradual increase of the hydrophobicity measured on the flat TiO_2 layers from 93.8° ± 0.5°, 102.3° ± 2.3°, 107.6° ± 4.0° to 120.3° ± 0.8° for 1 s, 1 and 5 min at RT, and 30 min at 60 °C, respectively (Figure 4e−h).

Interestingly, for the flat layers treated at RT, we observe a shift to higher binding energies in both the CF_2 and CF_3 peaks (≈0.35 ± 0.10 eV) and the F 1s peaks (≈0.30 ± 0.10 eV), while for the NTs, these shifts are smaller and disappear already for the 5 min RT treatment. These aspects may indicate differences in the ordering of the monolayer, which is tighter on the flat layers. The NT morphology allows for a different ordering, taking into account the inner and outer parts of the tube walls at the top of the surface. The F/Ti and P/Ti ratios (Figure 4l), clearly show that for the NT layers, in 5 min at RT, similar ratios are obtained as for 30 min at 60 °C (namely, F/Ti of 9.4 vs. 9.6, or P/Ti of 0.27 vs. 0.25). From the point of view of the FS bound on the top TiO_2 surface, for the NTs, 5 min is enough to bind a similar amount of FS. Considering the P/Ti ratio of NTs', which is 0.152 for the bare NTs and increases to 0.217 after 1 min FS decoration, this means that the amount of P is increased in the first 10 nm (surface sensitivity of XPS), compared to the bare NTs. While similar F/Ti ratios are obtained for the 1 min flat and NTs layers (5.4−5.7), and similar P/Ti ratios (considering that the NTs already contain some P from the anodizing electrolyte), the WCAs show an improved hydrophobicity for the NT morphology.

To follow up on these differences, the detailed examination of the C 1s and F 1s peaks for the 1 s and 1 min FS decorated samples was necessary, to evaluate the differences between a flat and NT morphology as shown in Figure 4m,n for 1 min and Figure S5 for 1 s. The peak fits further confirm the presence of the CF_2 and CF_3 groups of the FS (in both the C

https://doi.org/10.1021/acs.langmuir.4c04320
Langmuir 2025, 41, 1868−1875

1s and F 1s spectra), along with that of adventitious carbon, C−O and C−O−P bonds, or C═O bonds.

To summarize in the case of the C 1s peak fit, this includes (*i*) C−C, C−H bonds at ≈285.2 eV (including adventitious carbon contribution), (*ii*) C−O and C−O−P bonds at ≈286.8 eV, (*iii*) C═O bonds at ≈288.9 eV, (*iv*) CF_2 groups at 292.4 eV for flat and 292.0 eV for NTs, and (*v*) CF_3 groups at 294.4 eV for flat and 294.1 eV for NTs. The peak positions are in agreement with data in the literature,[6,35] and the peaks are visible for both the flat and NT layers, e.g., with 60 and 50% of the C coming from the CF_2/CF_3 groups, respectively, for the 1 min FS decorated layers. Similarly, different F contributions are also observed in the F 1s peak fits (Figure 4n), for the flat layers, CF_2 peak at ≈689.7 eV and CF_3 at ≈691.6 eV (with 87.5% and 12.5% of the peak area, respectively), which show a ≈0.3 eV shift to higher binding energies compared to the NT layers. For the NTs, these peaks are at ≈689.3 eV and ≈691.3 eV, with an additional metal fluoride peak at ≈684.8 eV (92.1%, 3.6%, and 4.4%, respectively). For the FS molecule, the ratio of the CF_2 to CF_3 groups from the molecular formula is between 5−9 to 1. Thus, the smaller peak intensity observed for CF_3 groups for the NTs may indicate that some existing groups are outside the depth sensitivity of the XPS, and thus inside the tube diameter or outside the tube wall.

CONCLUSIONS

In conclusion, we demonstrated the rapid self-assembly kinetics of fluorinated phosphate ester used to reduce the surface energy of flat and nanostructured metal oxides. The wet chemical approach allows the formation of hydrophobic coatings capable of trapping air underwater, achieving WCAs above 150° within minutes on rough TiO_2 NTs. The phosphate ester headgroup has no tendency to cross-link, allowing the FS solution to be used repeatedly for years without degradation. X-ray photoelectron spectroscopy confirmed the binding kinetics over different immersion times and temperatures, particularly between flat and NT morphologies, with the latter showing rapid and stable coating formation at ambient conditions. This work addresses critical challenges in the scalability, and efficiency of underwater aerophilicity, and provides an easy-to-implement, rapid, efficient, repeatable, scalable, cost-effective, and waste-free process to reduce the energy of solid surfaces. In addition, the proposed coating process is independent of substrate geometry and is equally effective in coating external and internal surfaces, small and large parts.

ASSOCIATED CONTENT

Supporting Information

The Supporting Information is available free of charge at https://pubs.acs.org/doi/10.1021/acs.langmuir.4c04320.

(1) ATR-FTIR spectra of bare and FS-coated TiO_2 NTs in the area of CH_2 stretching vibrations, (2) XPS survey spectra of flat and NT array substrates, (3) High-resolution XPS spectra of bare and functionalized flat and NT arrays for the O 1s and Ti 2p, (4) Atomic percentage data obtained from XPS, (5) Example of peak fitting of O 1s and Ti 2p for the 1 min FS decorated NT array, (6) C 1s and F 1s peak fittings for the 1 s FS decorated flat or NT layers (PDF)

Water affinity of the fluorinated for either 1 min at room temperature or 30 min at 60 °C TiO_2 NT samples (MP4)

AUTHOR INFORMATION

Corresponding Authors

Anca Mazare − *Department of Materials Science, Institute for Surface Science and Corrosion, Friedrich-Alexander-Universität Erlangen−Nürnberg, Erlangen 92058, Germany*; Email: anca.mazare@fau.de

Alexander B. Tesler − *Department of Physics, Chair of Biophysics, Friedrich-Alexander-Universität Erlangen−Nürnberg, Erlangen 92054, Germany*; orcid.org/0000-0003-3425-7667; Email: alexander.tesler@fau.de

Authors

Mahmut Hakan Ulubas − *Department of Materials Science, Institute for Surface Science and Corrosion, Friedrich-Alexander-Universität Erlangen−Nürnberg, Erlangen 92058, Germany*

Hyesung Kim − *Department of Materials Science, Institute for Surface Science and Corrosion, Friedrich-Alexander-Universität Erlangen−Nürnberg, Erlangen 92058, Germany*

Iana Fomicheva − *Department of Physics, Chair of Experimental Physics, Friedrich−Alexander Universität Erlangen−Nürnberg, Erlangen 91058, Germany*

George Sarau − *Fraunhofer Institute for Nanotechnology and Correlative Microscopy eV INAM, Forchheim 91301, Germany; Fraunhofer Institute for Ceramic Technologies and Systems IKTS, Forchheim 91301, Germany; Max Planck Institute for the Science of Light, Erlangen 91058, Germany*

Silke H. Christiansen − *Fraunhofer Institute for Nanotechnology and Correlative Microscopy eV INAM, Forchheim 91301, Germany; Fraunhofer Institute for Ceramic Technologies and Systems IKTS, Forchheim 91301, Germany; Institute for Experimental Physics, Freie Universität Berlin, Berlin 14195, Germany*; orcid.org/0000-0002-4908-4087

Wolfgang H. Goldmann − *Department of Physics, Chair of Biophysics, Friedrich-Alexander-Universität Erlangen−Nürnberg, Erlangen 92054, Germany*; orcid.org/0000-0003-0738-2665

Complete contact information is available at: https://pubs.acs.org/10.1021/acs.langmuir.4c04320

Author Contributions

The manuscript was written with contributions from all authors. All authors approved the final version of the manuscript.

Notes

The authors declare no competing financial interest.

ACKNOWLEDGMENTS

A.B.T. thanks the Deutsche Forschungsgemeinschaft (DFG) (award number 540989797) for financial support. A.B.T. and W.H.G. thank the Deutsche Forschungsgemeinschaft (DFG) (award number 442826449) for financial support. I.F., G.S., and S.C. were supported by the European Union's H2020 research and innovation program under the Marie Sklodowska-Curie grant agreement AIMed ID: 861138, by the European Union within the research projects 4D+ nanoSCOPE ID:

810316, LRI ID: C10, STOP ID: 101057961, by the German Research Foundation (DFG) within the research project UNPLOK ID: 523847126, and from the "Freistaat Bayern" and European Union within the project Analytiktechnikum für Gesundheits- und Umweltforschung AGEUM, StMWi-43-6623-22/1/3.

REFERENCES

(1) Rapoport, L.; Emmerich, T.; Varanasi, K. K. Capturing Bubbles and Preventing Foam Using Aerophilic Surfaces. *Adv. Mater. Interfaces* **2020**, *7* (6), 1901599.
(2) Shirtcliffe, N. J.; McHale, G.; Newton, M. I.; Perry, C. C.; Pyatt, F. B. Plastron properties of a superhydrophobic surface. *Appl. Phys. Lett.* **2006**, *89* (10), 104106.
(3) Barthlott, W.; Mail, M.; Neinhuis, C. Superhydrophobic hierarchically structured surfaces in biology: evolution, structural principles and biomimetic applications. *Philos. Trans. R. Soc. A* **2016**, *374* (2073), 20160191.
(4) Barthlott, W.; Schimmel, T.; Wiersch, S.; Koch, K.; Brede, M.; Barczewski, M.; Walheim, S.; Weis, A.; Kaltenmaier, A.; Leder, A.; Bohn, H. F. The Salvinia Paradox: Superhydrophobic Surfaces with Hydrophilic Pins for Air Retention Under Water. *Adv. Mater.* **2010**, *22* (21), 2325−2328.
(5) Jokinen, V.; Kankuri, E.; Hoshian, S.; Franssila, S.; Ras, R. H. A. Superhydrophobic Blood-Repellent Surfaces. *Adv. Mater.* **2018**, *30* (24), 1705104.
(6) Tesler, A. B.; Kolle, S.; Prado, L. H.; Thievessen, I.; Böhringer, D.; Backholm, M.; Karunakaran, B.; Nurmi, H. A.; Latikka, M.; Fischer, L.; Stafslien, S.; Cenev, Z. M.; Timonen, J. V. I.; Bruns, M.; Mazare, A.; Lohbauer, U.; Virtanen, S.; Fabry, B.; Schmuki, P.; Ras, R. H. A.; Aizenberg, J.; Goldmann, W. H. Long-term stability of aerophilic metallic surfaces underwater. *Nat. Mater.* **2023**, *22* (12), 1548−1555.
(7) Xiong, Z.; Yu, H.; Gong, X. Designing Photothermal Superhydrophobic PET Fabrics via In Situ Polymerization and 1,4-Conjugation Addition Reaction. *Langmuir* **2022**, *38* (28), 8708−8718.
(8) Rasitha, T. P.; Krishna, N. G.; Anandkumar, B.; Vanithakumari, S. C.; Philip, J. A comprehensive review on anticorrosive/antifouling superhydrophobic coatings: Fabrication, assessment, applications, challenges and future perspectives. *Adv. Colloid Interface Sci.* **2024**, *324*, 103090.
(9) Prado, L. H.; Hayek, S.; Mazare, A.; Erceg, I.; Sarau, G.; Christiansen, S.; Kamaleev, M.; Wurmshuber, M.; Lohbauer, U.; Goldmann, W. H.; Virtanen, S.; Tesler, A. B. Aerophilic Surfaces for Sustained Corrosion Protection of Metals Underwater. *Adv. Funct. Mater.* **2024**, *34*, 2407444.
(10) Shaikh, A.; Qu, J.; Grachev, D. The role of synthetic superhydrophobic surfaces in construction materials. *Cur. Trends Civil Struct. Eng.* **2020**, *6*, e000628.
(11) Li, L.; Wei, J.; Zhang, J.; Li, B.; Yang, Y.; Zhang, J. Challenges and strategies for commercialization and widespread practical applications of superhydrophobic surfaces. *Sci. Adv.* **2023**, *9* (42), No. eadj1554.
(12) Tesler, A. B.; Nurmi, H. A.; Kolle, S.; Prado, L. H.; Karunakaran, B.; Mazare, A.; Erceg, I.; de Brito Soares, C. D.; Sarau, G.; Christiansen, S.; Stafslien, S.; Alvarenga, J.; Aizenberg, J.; Fabry, B.; Ras, R. H. A.; Goldmann, W. H. Predicting plastron thermodynamic stability for underwater superhydrophobicity. *Commun. Mater.* **2024**, *5* (1), 112.
(13) Marmur, A.; Della Volpe, C.; Siboni, S.; Amirfazli, A.; Drelich, J. W. Contact angles and wettability: towards common and accurate terminology. *Surf. Innov.* **2017**, *5* (1), 3−8.
(14) Parvate, S.; Dixit, P.; Chattopadhyay, S. Superhydrophobic Surfaces: Insights from Theory and Experiment. *J. Phys. Chem. B* **2020**, *124* (8), 1323−1360.
(15) Akuoko, S. Y.; Kwon, K.-S. Fabrication and Applications of Nature-Inspired Surfaces with Selective Wettability. *Langmuir* **2024**, *40* (31), 15969−15995.
(16) Zeng, Q.; Zhou, H.; Huang, J.; Guo, Z. Review on the recent development of durable superhydrophobic materials for practical applications. *Nanoscale* **2021**, *13* (27), 11734−11764.
(17) Chen, X.; Zhong, L.; Gong, X. Robust Superhydrophobic Films Based on an Eco-Friendly Poly(l-lactic acid)/Cellulose Composite with Controllable Water Adhesion. *Langmuir* **2024**, *40* (19), 10362−10373.
(18) Zhang, Y.; Gong, X. Smart and durable pH-responsive superhydrophobic fabrics with switchable surface wettability for high-efficiency and complex oil/water separation. *Giant* **2023**, *14*, 100157.
(19) Paz, Y. Self-assembled monolayers and titanium dioxide: From surface patterning to potential applications. *Beilstein J. Nanotechnol.* **2011**, *2*, 845−861.
(20) Helmy, R.; Fadeev, A. Y. Self-Assembled Monolayers Supported on TiO_2: Comparison of $C_{18}H_{37}SiX_3$ (X = H, Cl, OCH_3), $C_{18}H_{37}Si(CH_3)_2Cl$, and $C_{18}H_{37}PO(OH)_2$. *Langmuir* **2002**, *18* (23), 8924−8928.
(21) Mazare, A.; Park, J.; Simons, S.; Mohajernia, S.; Hwang, I.; Yoo, J. E.; Schneider, H.; Fischer, M. J.; Schmuki, P. Black TiO_2 nanotubes: Efficient electrodes for triggering electric field-induced stimulation of stem cell growth. *Acta Biomater.* **2019**, *97*, 681−688.
(22) Owens, D. K.; Wendt, R. C. Estimation of the surface free energy of polymers. *J. Appl. Polym. Sci.* **1969**, *13* (8), 1741−1747.
(23) Park, J.; Cimpean, A.; Tesler, A. B.; Mazare, A. Anodic TiO_2 Nanotubes: Tailoring Osteoinduction via Drug Delivery. *Nanomaterials* **2021**, *11* (9), 2359.
(24) Cousins, I. T.; Johansson, J. H.; Salter, M. E.; Sha, B.; Scheringer, M. Outside the Safe Operating Space of a New Planetary Boundary for Per- and Polyfluoroalkyl Substances (PFAS). *Environ. Sci. Technol.* **2022**, *56* (16), 11172−11179.
(25) Kido, D.; Komatsu, K.; Suzumura, T.; Matsuura, T.; Cheng, J.; Kim, J.; Park, W.; Ogawa, T. Influence of Surface Contaminants and Hydrocarbon Pellicle on the Results of Wettability Measurements of Titanium. *Int. J. Mol. Sci.* **2023**, *24* (19), 14688.
(26) Park, J.; Tesler, A. B.; Gongadze, E.; Iglič, A.; Schmuki, P.; Mazare, A. Nanoscale Topography of Anodic TiO_2 Nanostructures Is Crucial for Cell-Surface Interactions. *ACS Appl. Mater. Interfaces* **2024**, *16* (4), 4430−4438.
(27) Filippin, N.; Castillo-Seoane, J.; López-Santos, M. C.; Rojas, C. T.; Ostrikov, K.; Barranco, A.; Sánchez-Valencia, J. R.; Borrás, A. Plasma-Enabled Amorphous TiO_2 Nanotubes as Hydrophobic Support for Molecular Sensing by SERS. *ACS Appl. Mater. Interfaces* **2020**, *12* (45), 50721−50733.
(28) Tesler, A. B.; Kim, P.; Kolle, S.; Howell, C.; Ahanotu, O.; Aizenberg, J. Extremely durable biofouling-resistant metallic surfaces based on electrodeposited nanoporous tungstite films on steel. *Nat. Commun.* **2015**, *6* (1), 8649.
(29) Claves, D. Spectroscopic study of fluorinated carbon nanostructures. *New J. Chem.* **2011**, *35* (11), 2477−2482.
(30) Ignatieva, L. N.; Mashchenko, V. A.; Zverev, G. A.; Ustinov, A. Y.; Slobodyuk, A. B.; Bouznik, V. M. Study of the manufactured copolymers of ethylene with tetrafluoroethylene. *J. Fluorine Chem.* **2020**, *231*, 109460.
(31) Withnall, R.; Andrews, L. Infrared spectra of oxygen atom-phosphine reaction products trapped in solid argon. *J. Phys. Chem.* **1988**, *92* (16), 4610−4619.
(32) Ron, H.; Rubinstein, I. Self-Assembled Monolayers on Oxidized Metals. 3. Alkylthiol and Dialkyl Disulfide Assembly on Gold under Electrochemical Conditions. *J. Am. Chem. Soc.* **1998**, *120* (51), 13444−13452.
(33) Mazare, A.; Hwang, I.; Tesler, A. B. Surface modification of TiO2 nanotubes via pre-loaded hydroxyapatite towards enhanced bioactivity. *Mater. Today Commun.* **2024**, *39*, 109216.
(34) Moulder, J. F.; Chastain, J. *Handbook of X-ray Photoelectron Spectroscopy: A Reference Book of Standard Spectra for Identification and*

https://doi.org/10.1021/acs.langmuir.4c04320
Langmuir 2025, 41, 1868−1875

Interpretation of XPS Data; Physical Electronics Division, Perkin-Elmer Corporation, 1992.
(35) Crist, B. V. *Handbooks of Monochromatic XPS Spectra: Vol. 4: Polymers and Polymers Damaged by X-rays*; XPS International LLC, 2004.

https://doi.org/10.1021/acs.langmuir.4c04320
Langmuir 2025, 41, 1868−1875